Analysis and Design of Parallel Mechanisms with Flexure Joints

Byoung Hun Kang, John T. Wen
Center for Automation Technologies
Rensselaer Polytechnic Institute
Troy, NY 12180.
Emails: {kangb,wen}@cat.rpi.edu

Nicholas G. Dagalakis, Jason J. Gorman
Intelligent Systems Division
National Institute of Standards and Technology
Gaithersburg, MD 20899, USA
Emails: {dagalaki,gorman}@cme.nist.gov

***Abstract*— Flexure joints are frequently used in precision motion stages and micro-robotic mechanisms due to their monolithic construction. The joint compliance, however, can affect the static and dynamic performance of the overall mechanism. In this paper, we consider the analysis and design of general platform type parallel mechanisms containing flexure joints. We consider static performance measures such as task space stiffness and manipulability, while subject to constraints such as joint stress, mechanism size, workspace volume, and dynamic characteristics. Based on these performance measures and constraints, we adopt the multi-objective optimization approach. We first obtain the Pareto frontier, which can then be used to select the desired design parameters based on secondary criteria such as performance sensitivity. To simplify presentation, we consider only lumped approximation of flexure joints in the pseudo-rigid-body approach. A planar mechanism is included to illustrate the analysis and design techniques. Tools presented in this paper can also be applied to a broader class of compliant mechanisms, including robots with inherent joint flexibility as well as compliant robots for contact tasks.**

I. Introduction

Flexure joints have been used in precision instruments such as watches and clocks for hundreds of years, and continue to be used today in applications such as optical systems, micro-robots, and clean room equipment. Flexure joints offer significant advantages over conventional joints [1], [2] in terms of both manufacturing and operational characteristics. Mechanically assembled joints inevitably reduce accuracy due to manufacturing tolerances. Flexure joints are typically manufactured monolithically and therefore avoid assembly errors. The monolithic construction also implies a relatively easy manufacturing process and potentially very compact design. In terms of operation, flexure joints have little friction losses and do not require lubrication. They generate smooth and continuous displacement without backlash. With a suitable choice of material, flexure joints exhibit a predictable and repeatable relationship between force and displacement. These attributes have endeared flexure mechanisms to meso- and micro-scale precision motion applications, from optical stages to micro-electro-mechanical-systems (MEMS).

Thorough treatments on the characterization and design of flexure joints and mechanisms may be found in [1], [3]. Flexure mechanism design is usually addressed either from a kinematic synthesis point of view with the overall mechanism compliance as a secondary criterion, or from the compliance point of view [1] with the emphasis on synthesizing desired compliance characteristics using, for example, topological optimization [4], [5] or finite element analysis [6], [7]. The general problem of compliance synthesis has been addressed using simple springs [8] with specific solutions proposed for torsional and line springs in [9]–[11]. However, such an approach has several drawbacks: the design criterion only involves the desired compliance; constraints are not taken into account; and the overall mechanism is passive without consideration of actuators. The specific problem of synthesizing a desired grasp compliance by choosing appropriate finger compliance is used in [12]. Independent of joint compliance, optimization based design methods have also been developed for parallel mechanisms [13], [14], but the joint compliance is not taken into account. The goal of this paper is to present analysis and design tools for parallel mechanisms containing flexure joints based on the pseudo-rigid-body model. Our approach is to balance the motion and compliance consideration through a multi-objective optimization.

A well established criterion for assessing the behavior of a serial or parallel manipulator is the manipulability ellipsoid which is the task space image of a ball in the active joint velocity space. This concept was first proposed for serial manipulators [15] and later extended to parallel robots [16], [17]. We pose the design problem as a multi-objective optimization problem with the performance metrics based on manipulability and stiffness subject to constraints (such as the maximum joint stress, workspace, mechanism size, etc.) and bounds on the design parameters. The Pareto frontier [18] is then calculated and the final design determined based on secondary considerations such as dynamic characteristics and performance sensitivity. As an example, we include a 1-D stage designed by the National Institute of Standards and Technology (NIST) to illustrate the modeling and design approach described in the paper.

II. Differential Kinematics

Consider a parallel mechanism with active joints denoted by the vector q_a and passive joints denoted by q_p. The differential

kinematics may be described as

$$\begin{bmatrix} \Delta x_T \\ 0 \end{bmatrix} = \underbrace{\begin{bmatrix} J_{T_a} & J_{T_p} \\ J_{C_a} & J_{C_p} \end{bmatrix}}_{J:=\begin{bmatrix} J_T \\ J_C \end{bmatrix}} \underbrace{\begin{bmatrix} \Delta q_a \\ \Delta q_p \end{bmatrix}}_{\Delta q} \tag{1}$$

For parallel mechanisms with conventional passive joints, J_{C_p} is typically square (same number of passive joints as constraints) so that there are no undesirable internal constraint forces. It is also essential to ensure that J_{C_p} is invertible so that there would not be undesired motion (this is the kinematic stability condition). If J_{C_p} is a tall matrix, the mechanism is overconstrained and it cannot move unless some of the constraints are redundant. If this is the case for a working mechanism, the rigid body kinematic description is not adequate, and either more lumped joints need to be added or a distributed description should be used. If J_{C_p} is a fat matrix, the mechanism is underconstrained. For conventional parallel mechanisms, this is not desirable, since there could be uncontrolled motion resulting from disturbances. However, we shall see that for flexure mechanisms, this may be acceptable provided that the stiffness in the direction of unwanted motion is sufficiently large.

We now consider a fully constrained mechanism (when active joints are locked) or underconstrained mechanism, i.e., J_{C_p} is square or fat, and full rank. If J_{C_p} is fat, Δq_p cannot be uniquely solved since any vector in the null space of J_{C_p} may be added to the solution. In this case, we assume that the solution Δq_p minimizes the strain energy in the passive joints, i.e., Δq_p is found from

$$\min_{\Delta q_p} \frac{1}{2} \Delta q_p^T K_{q_p} \Delta q_p, \text{ subject to } 0 = J_{C_a} \Delta q_a + J_{C_p} \Delta q_p, \tag{2}$$

where we have assumed linear spring characteristics with spring constant K_{q_p}. We treat Δq_p as the actual joint displacement since we assume that the joint displacement from the equilibrium is small. The solution of (2) may be readily found:

$$\Delta q_p = -J_{C_p}^{\ddagger} J_{C_a} \Delta q_a \tag{3}$$

where

$$J_{C_p}^{\ddagger} := K_{q_p}^{-1/2} (J_{C_p} K_{q_p}^{-1/2})^{\dagger} \tag{4}$$

and † denotes the Moore-Penrose pseudo-inverse. If J_{C_p} is square invertible, then $J_{C_p}^{\ddagger} = J_{C_p}^{-1}$.

The relationship between active joint displacement and task displacement is then:

$$\Delta x_T = \underbrace{(J_{T_a} - J_{T_p} J_{C_p}^{\ddagger} J_{C_a})}_{:=J_{T_{comp}}} \Delta q_a. \tag{5}$$

By applying the principle of virtual work, we obtain the dual relationship:

$$\underbrace{\begin{bmatrix} \tau_a \\ \tau_p \end{bmatrix}}_{\tau} = \begin{bmatrix} J_{T_a}^T & J_{C_a}^T \\ J_{T_p}^T & J_{C_p}^T \end{bmatrix} \begin{bmatrix} f_T \\ f_C \end{bmatrix}, \tag{6}$$

where f_T is the externally applied spatial force, f_C is the constraint spatial force (to enforce the kinematic constraint, the bottom portion of (1)), τ_a and τ_p are the torque vectors applied at the active and passive joints, respectively. When the passive joints are free (e.g., pin, spherical, etc.), $\tau_p = 0$. However, for flexure joints, τ_p is related to Δq_p.

By far the most common configuration of parallel mechanism is a platform supported by multiple legs. For an M-leg platform mechanism, the differential kinematics may be written as

$$\Delta x_T = J_{T1} \Delta q_{a1} + J_{C1} \Delta q_{p1} = \ldots = J_{TM} \Delta q_{aM} + J_{CM} \Delta q_{pM}. \tag{7}$$

We can rewrite this relation as

$$\underbrace{\begin{bmatrix} J_{a1} & & 0 & & & \\ & \ddots & & & 0 & \\ & & J_{aM} & & & \\ & & & J_{p1} & & \\ & 0 & & & \ddots & \\ & & & & & J_{pM} \end{bmatrix}}_{J} \begin{bmatrix} \Delta q_{a1} \\ \ldots \\ \Delta q_{aM} \\ \Delta q_{p1} \\ \ldots \\ \Delta q_{pM} \end{bmatrix}$$

$$= \begin{bmatrix} \Delta x_1 \\ \ldots \\ \Delta x_M \end{bmatrix} = \underbrace{\begin{bmatrix} I \\ \ldots \\ I \end{bmatrix}}_{A} \Delta x_T. \tag{8}$$

Since A is of full column rank, we can immediately transform this to the form (1):

$$\Delta x_T = A^{\dagger} J \Delta q \tag{9}$$

$$0 = \widetilde{A} J \Delta q \tag{10}$$

where $A^{\dagger}$ is the pseudo-inverse of A and $\widetilde{A}$ is a full row rank matrix whose null space coincides with the column space of A.

III. Performance Measures

A. Manipulability

Manipulability is characterized by $J_{T_{comp}}$ as in (5). Depending on the design objective, different metrics may be imposed.

If it is desirable to have an isotropic mechanism (the task frame is equally easy to move in all directions, for active joint motion constrained in a unit ball), then the metric to minimize may be

$$\mu_M(J_{T_{comp}}) = \left(\frac{s_{\max}(J_{T_{comp}})}{s_{\min}(J_{T_{comp}})} - 1\right)^2 \tag{11}$$

where $s_{\min}$ and $s_{\max}$ denote the minimum and maximum singular values, respectively (equivalently, the lengths of the principal major and minor axes of the manipulability ellipsoid).

It may also be desirable to maximize the overall workspace. In this case, we can choose to maximize the volume of the manipulability ellipsoid by minimizing the metric

$$\mu_M(J_{T_{comp}}) = \left(\prod_j s_j(J_{T_{comp}}) \right)^{-1}. \tag{12}$$

If it is desired to increase manipulability in directions given by the unit vectors $\{u_i\}$ and decrease manipulability in directions given by $\{v_i\}$, then a possible metric to minimize is the following weighted sum:

$$\begin{aligned}\mu_M(J_{T_{comp}}) &= \sum_i \alpha_i \left(u_i^T J_{T_{comp}}^T J_{T_{comp}} u_i\right)^{-1} \\ &\quad + \sum_i \beta_i \left(v_i^T J_{T_{comp}}^T J_{T_{comp}} v_i\right). \quad (13)\end{aligned}$$

B. Maximum Joint Stress

The maximum stresses in the flexure joints are approximately proportional to the maximum deflections of these joints. For example, for a circular notch hinge joint with radius R, hinge width t, and Young's Modulus E, the maximum stress, $\sigma_{\max}$, is related to the angular deflection, $\theta_{\max}$, by [3]

$$\theta_{\max} = \frac{3\pi}{4E}\sqrt{\frac{R}{t}}\sigma_{\max}. \quad (14)$$

For a cantilevered joint with length L and width t, the relationship is approximately

$$\theta_{\max} = \frac{0.148}{E}\frac{L}{t}\sigma_{\max}. \quad (15)$$

If the maximum joint stress is given (e.g., from the yield stress of the material), it can be converted to an equivalent maximum joint displacement, $\Delta q_p^{(\max)}$ by using the above formulas. The max joint stress constraint can then be stated as a maximum deflection constraint:

$$|\Delta q_p| \le \Delta q_p^{(\max)}, \quad (16)$$

where $|\cdot|$ and $\le$ are treated in the componentwise sense.

C. Task Space Stiffness

The task space stiffness is defined from the force balance between the applied external spatial force f_T and the corresponding task frame displacement Δx_T:

$$f_T = K_T \Delta x_T. \quad (17)$$

Rewrite the force balance equation (6) as

$$\tau = J_T^T f_T + J_C^T f_C. \quad (18)$$

By assumption, J_{C_p} is full row rank, therefore, J_C is full row rank. Let $\widetilde{J_C}$ be the full column rank matrix whose column space coincides with the null space of J_C. Then

$$\widetilde{J_C}^T \tau = \widetilde{J_C}^T J_T^T f_T. \quad (19)$$

Substituting in (17) and using the differential kinematics (top portion of (1)), we get

$$\begin{aligned}\widetilde{J_C}^T \tau &= \widetilde{J_C}^T J_T^T K_T \Delta x_T \\ &= \widetilde{J_C}^T J_T^T K_T J_T \Delta q. \quad (20)\end{aligned}$$

Assume the joint torque is related to the joint displacement through a linear spring relationship:

$$\begin{bmatrix} \tau_a \\ \tau_p \end{bmatrix} = \underbrace{\begin{bmatrix} K_{q_a} & 0 \\ 0 & K_{q_p} \end{bmatrix}}_{K_q} \begin{bmatrix} \Delta q_a \\ \Delta q_p \end{bmatrix}, \quad (21)$$

where K_{q_a} denotes the active joint stiffness and K_{q_p} denotes the passive joint stiffness. If proportional-derivative type of feedback is used for the active joints, then

$$K_{q_a} = K_{q_a}^{(p)} + K_{q_a}^{(a)} \quad (22)$$

where $K_{q_a}^{(p)}$ denotes the passive portion and $K_{q_a}^{(a)}$ denotes the proportional feedback gain.

Substituting (21) into (20), we get

$$\begin{aligned}\widetilde{J_C}^T K_q \Delta q &= \widetilde{J_C}^T J_T^T K_T \Delta x_T \\ &= \widetilde{J_C}^T J_T^T K_T J_T \Delta q. \quad (23)\end{aligned}$$

From the kinematic constraint (bottom portion of (1)), we know Δq may be expressed as

$$\Delta q = \widetilde{J_C}\phi \quad (24)$$

for some vector ϕ. Substituting into (23), we get

$$\widetilde{J_C}^T K_q \widetilde{J_C}\phi = \widetilde{J_C}^T J_T^T K_T J_T \widetilde{J_C}\phi. \quad (25)$$

Since this holds for any ϕ, we obtain the expression for the task space stiffness

$$\widetilde{J_C}^T K_q \widetilde{J_C} = \widetilde{J_C}^T J_T^T K_T J_T \widetilde{J_C}. \quad (26)$$

If the mechanism is kinematically stable, i.e., J_{C_p} is square invertible, then

$$\widetilde{J_C} = \begin{bmatrix} I \\ -J_{C_p}^{-1} J_{C_a} \end{bmatrix}, \quad (27)$$

and (26) becomes

$$K_{q_a} + J_{C_a}^T J_{C_p}^{-T} K_{q_p} J_{C_p}^{-1} J_{C_a} = J_{T_{comp}}^T K_T J_{T_{comp}}, \quad (28)$$

which is the same expression as obtained in [19].

For a circular notch hinge type of flexure joint (see Fig. 1(a)), the joint stiffness modeled as a pure rotation is given by [3]

$$K \approx \frac{2Ep}{9\pi}\sqrt{\frac{t^5}{R}}, \quad (29)$$

where E is the Young's Modulus of the hinge material, p is the depth of the joint, t the thickness of the thinnest portion of the joint, and R is the radius of the circle. A full 3D (planar translation and rotation) joint stiffness model is also given in [3].

For a cantilevered joint (see Fig. 1(b)), the joint stiffness may be approximately modeled as

$$K \approx 2\gamma K_\theta \frac{EI}{L}, \quad (30)$$

where E is the Young's Modulus, $I = \frac{pt^3}{12}$ is the moment of inertia about the axis perpendicular to the joint, L is the

length of the joint and γ and K_θ are experimentally determined constants:

$$\gamma = 0.8517, K_\theta = 2.6762.$$

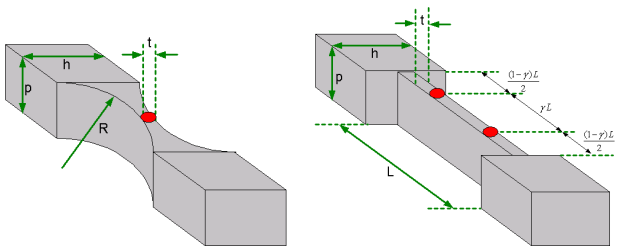

(a) Circular Notch Hinge Joint (b) Cantilevered Joint

Fig. 1. Flexure Joint Modeling

Similar to the manipulability matrix, different metrics may be used depending on the application. For example, in [19], the goal is to ensure the stiffness matrix is decoupled. In that case, the metric may be chosen to be

$$\mu_K(K_T) = \|K_T - \text{diag}(K_T)\| . \tag{31}$$

If maximum stiffness is desired, the metric may involve maximizing the volume of K_T or minimizing its reciprocal:

$$\mu_K(K_T) = \left(\prod_j s_j(K_T) \right)^{-1} . \tag{32}$$

If it is desired to increase stiffness in directions given by the unit vectors $\{u_i\}$ and decrease stiffness in directions given by $\{v_i\}$, a possible metric to minimize is the following weighted sum:

$$\mu_K(J_{T_{comp}}) = \sum_i \alpha_i \left(u_i^T K_T u_i \right)^{-1} + \sum_i \beta_i \left(v_i^T K_T v_i \right) . \tag{33}$$

IV. Example: NIST 1-D Stage

A. Mechanism Architecture

A 1-degree-of-freedom (DOF) macro-scale precision motion stage using flexure joints was designed and fabricated by NIST [20], [21]. Several meso-scale (about the size of a credit card) models have also been built [22]. A schematic of the mechanism is shown in Fig. 2. A piezoelectric actuator transmits the y-axis motion through joints 1 and 4 to the two lower arms. These arms pivot about joints 2 and 5 and move the output stage through joints 3 and 6. To support the output stage (and to reduce the angular crosstalk, i.e., undesirable angular motion), two additional arms also support the platform through joints 7-10. The goal of the design is to achieve desired manipulability (pure translation in y) and stiffness (large stiffness in the angular and x directions). The joints are constructed as circular notch joints (see Fig. 3 from [20]). However, depending on the exact joint model used, the design result would be different. This is discussed in the next section. By replicating the design along the orthogonal axis, a 2-DOF version has also been designed and built. Such stages are currently being considered for satellite optical communication [23].

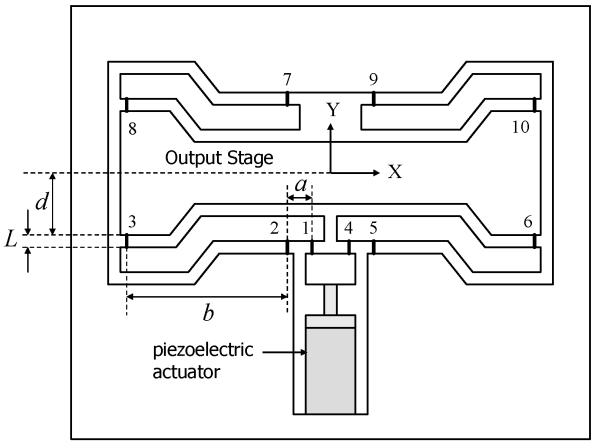

Fig. 2. Schematic of NIST 1-D Mechanism

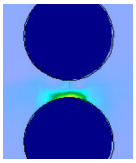

Fig. 3. Flexure Joint in NIST 1-D Mechanism

B. Kinematic Models

The mechanism consists of 6 kinematic chains constrained at the platform. This means that there are 15 total constraints (5 loops involving (x, y, θ)).

If all the joints in Fig. 2 are chosen to be idealized 1D rotational joints, then there are 10 passive DOF's and the mechanism is overconstrained (J_{C_p} is 15×10). Indeed, in this case, the mechanism cannot move from the equilibrium position shown. This means that the 1D joint approximation is not adequate to describe this mechanism.

There are a number of possible modifications that we could introduce. At this point, we do not know which model matches closest with the physical mechanism; we intend to conduct calibration tests at NIST in the near future. To illustrate the design procedure, we have considered the following two joint models:

- **A**: Replace joints 1, 3, 4, 6, 8, 10 by two rotational joints connected by a short rigid segment (cantilevered joint model). The motivation of this assumption is to allow rotation as well as shear type of translation at these joints. Joints 2, 5, 7, 9 serve as pivots and are retained as pure rotational joints (circular notch joint model). In this case, there are 16 passive joints and 15 constraints, i.e., $\widetilde{J_C}$ is rank 2 (including one active joint). Since $J_T \widetilde{J_C}$ (in (26)) is rank 2, only the x-y components of K_T can be determined.

- **B**: Replace all joints by double joints (cantilevered joint model). Now there are 20 passive joints and 15 constraints, and K_T may be fully determined.

The flexure mechanism is made from 6061-T6 Aluminum alloy. The Young's Modulus is $E = 70$ GPa. The four quadrants of the stage are nominally all symmetric. We use the following dimensions:

$$a = 1.5 \text{ mm}, b = 15 \text{ mm}, L = 0.425 \text{ mm}, d = 8.625 \text{ mm}.$$

For circular notch joints, the passive joint stiffness is calculated using (29) with $r = \frac{L}{2} = 0.2125$ mm, $t = 0.1$ mm, $p = 6.35$ mm:

$$K_p = 0.2140 \text{ N-m/rad}.$$

For cantilevered joints, the passive joint stiffness is calculated using (30) with $L = 0.25$ mm, $t = 0.1$ mm, and $p = 6.35$ mm:

$$K_p = 0.6701 \text{ N-m/rad}.$$

The actuator stiffness is obtained from [22]:

$$K_a = 2.1569 \times 10^7 \text{ N/m}.$$

In both cases A and B, the task space Jacobian is (the task coordinate is arranged as (θ, x, y)):

$$J_{T_{comp}} = \begin{bmatrix} 0 \\ 0 \\ -9.9998 \end{bmatrix},$$

showing only y-direction motion of the task frame.

The x-y portion of K_T in Case A is almost diagonal:

$$K_{T(x,y)} = \begin{bmatrix} 1.4100 \times 10^9 & -6.7705 \times 10^{-5} \\ -6.7705 \times 10^{-5} & 7.2841 \times 10^5 \end{bmatrix} \text{N/m}$$

with eigenvalues $(1.4100 \times 10^9, 7.2841 \times 10^5)$. The full K_T in Case B is

$$K_T = \begin{bmatrix} 6.9911 \times 10^{25} & 3.1518 \times 10^{16} & 2.4655 \times 10^{15} \\ 3.1518 \times 10^{16} & 8.3672 \times 10^8 & 1.1115 \times 10^6 \\ 2.4655 \times 10^{15} & 1.1115 \times 10^6 & 6.4209 \times 10^5 \end{bmatrix},$$

which shows very high stiffness in the rotational direction. The eigenvalues are $(6.9911 \times 10^{25}, 8.2251 \times 10^8, 5.5514 \times 10^5)$ with eigenvectors almost perfectly aligned with the unit vectors. The order of stiffness values in the x and y directions for Cases A and B are very close, demonstrating consistency between the two approaches.

C. Design Optimization

To illustrate the design optimization procedure, we choose to maximize the manipulability (along y) and the relative stiffness between the x and y directions:

$$\text{Manipulability: } \mu_1 = \frac{1}{\left\| J_{T_{comp}} \right\|} \tag{34}$$

$$\text{Stiffness: } \mu_2 = \frac{10}{K_x/K_y}. \tag{35}$$

Note that the scaling constants are added to normalize between the two measures.

For the maximum joint stress, we use the yield stress for AL6061-T6: $\sigma_{\max} = 220$ MPa. The maximum stress constraint is imposed when the active joint is at its maximum extension $\Delta q_{a_{\max}} = 9.1$ μm. Eqs. (14) and (15) are used to calculate the joint stress for circular notch joints and cantilevered joints, respectively. In this case, the maximum allowed joint deflection for the circular notch joint is 0.6731° and for the cantilevered joint 0.1003°. The design parameters are chosen to be (a, b, c) with the bounds:

$$\begin{aligned} 0.5 \text{ mm} \leq \quad & a \quad \leq 4.5 \text{ mm}, \\ 5 \text{ mm} \leq \quad & b \quad \leq 45 \text{ mm}, \\ 0.08 \text{ mm} \leq \quad & L \quad \leq 0.75 \text{ mm}. \end{aligned}$$

The Pareto frontiers for cases A and B are shown in Figures 4–5. When the two performance indices are combined with equal weights:

$$\mu = 0.5\mu_1 + 0.5\mu_2,$$

the optimal solutions are shown in Table I with the optimal performance indices

$$\begin{aligned} \text{Case A}: \quad & \text{Manipulability } = 15.9717, \frac{K_x}{K_y} = 680.1686 \\ \text{Case B}: \quad & \text{Manipulability } = 13.9626, \frac{K_x}{K_y} = 915.0178. \end{aligned}$$

Compared with the nominal manipulability of 9.9998 and relative stiffness $\frac{K_x}{K_y} = 458.8294$, for both cases, the optimal solutions in both cases improve both μ_1 and μ_2, with Case B showing the greater improvement. However, the absolute stiffness in the x direction is reduced by a factor of 10. If this is not acceptable, K_x may be added as an additional performance measure or a design constraint. The maximum passive joint deflections range from 0.1880° to 0.6731° for Case A and Case B, well within the maximum deflection constraint for circular notch joint.

	Initial value	Optimal value	
		Case A	Case B
a	1.5 mm	1.2 mm	1.3 mm
b	15 mm	18.6 mm	18.5 mm
L	0.425 mm	0.506 mm	0.379 mm

TABLE I
OPTIMAL DESIGN VALUES FOR CASE A AND CASE B

V. CONCLUSION

In this paper, we have presented analysis and design tools for parallel mechanisms with lumped flexure joints. The key difference between flexure mechanism and parallel mechanisms with conventional joints is that kinematic stability is no longer a design consideration. Instead, task space stiffness needs to be carefully designed to avoid undesired motion in the presence of external loads. We pose the design problem as a multi-objective optimization with manipulability and stiffness as performance measures and maximum joint stress and design

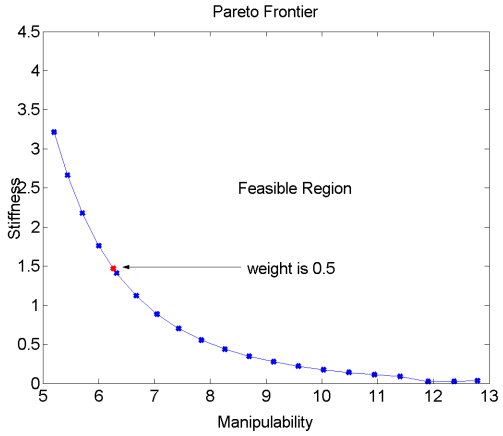

Fig. 4. Pareto Frontier for Case A

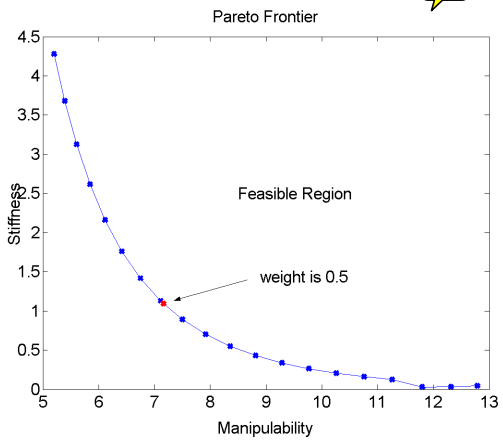

Fig. 5. Pareto Frontier for Case B

parameter bounds as constraints. A 1-D stage designed by NIST is used as an example to illustrate the modeling and design approach. It is also shown that by making different joint assumptions, e.g., a single circular notch joint vs. a bending beam joint modeled as a double flexure, the optimal solution could be quite different. We are currently planning to conduct experimental trials at NIST to determine the validity of the models and also fabricate new stages based on the optimization results.

ACKNOWLEDGMENT

This research is conducted based in part on the support by the National Science Foundation under Grant IIS-9820709. This work is also supported in part by the Center for Automation Technologies under a block grant from the New York State Office of Science, Technology, and Academic Research.

REFERENCES

[1] L.L. Howell. *Compliant Mechanisms*. John Wiley and Sons, Inc., 2001.

[2] S. Kota. Compliant systems using monolithic mechanisms. *Smart Material Bulletin*, pages 7–9, March 2000.

[3] S.T. Smith. *Flexure: Elements of Elastic Mechanisms*. Gordon and Breach Science Publishers, 2000.

[4] S. Kota, J. Joo, Z. Li, S.M. Rodgers, and J. Sniegowski. Design of compliant mechanisms: Applications to MEMS. *Analog Integrated Circuits and Signal Processing*, 29:7–15, 2001.

[5] G.K. Ananthasuresh and M. Frecker. Synthesis of compliant mechanisms using continuum models. In L. Howell, editor, *Compliant Mechanisms*. John Wiley and Sons, Inc., 2001.

[6] M.L. Culpepper and G. Anderson. Design of a low-cost nano-manipulator which utilizes a monolithic, spatial compliant mechanism. *Submitted to the Journal of Precision Engineering*, 2003.

[7] H.H. Pham and I.-M. Chen. Optimal synthesis for workspace and manipulability of parallel flexure mechanism. In *11th World Congress in Mechanism and Machine Science*, Tianjin, China, 2003.

[8] J. Loncaric. *Geometrical Analysis of Compliant Mechanisms in Robotics*. PhD thesis, Harvard University, 1985.

[9] S. Huang and J. M. Schimmels. Achieving an arbitrary spatial stiffness with springs connected in parallel. *J. Mech. Design*, 120(4):520–526, 1998.

[10] N. Ciblak and H. Lipkin. Synthesis of stiffness by springs. In *Proceedings of 1998 ASME Design Engineering Technical Conferences*, Atlanta, GA, September 1998.

[11] R.G. Roberts. Minimal realization of a spatial stiffness matrix with simple springs connected in parallel. *IEEE Transaction on Robotics and Automation*, 15(5):953–958, October 1999.

[12] T.G. Sugar and V. Kumar. Design and control of a complaint parallel manipulator. *ASME Journal of Mechanical Design*, December 2002.

[13] Y.J. Lou, G.F. Liu, and Z.X. Li. Optimal design of parallel manipulators via LMI approach. In *Proceedings of the 2003 IEEE International Conference on Robotics & Automation*, pages 1869–1874, Taipei, Taiwan, September 2003.

[14] J.-P. Merlet. Determinination of the optimal geometry of modular parallel robots. In *Proceedings of the 2003 IEEE International Conference on Robotics & Automation*, pages 1197–2002, Taipei, Taiwan, September 2003.

[15] T. Yoshikawa. Manipulability of robotic mechanisms. *International Journal of Robotics Research*, 4(2):3–9, 1985.

[16] J. T. Wen and L. S. Wilfinger. Kinematic manipulability of general constrained rigid multibody systems. *IEEE Transactions on Robotics and Automation*, 15(3):558–567, 1999.

[17] A. Bicchi and D. Prattichizzo. Manipulability of cooperation robots with passive joints. In *Proc. 1997 IEEE Int. Conf. on Robotics and Automation*, pages 1038–1044, 1998.

[18] A. Ismail-Yahaya and A. Messac. Required relationship between objective function and pareto frontier orders:practical implications. *American Institute of Aeronautics and Astronautics Journal*, 39(11):2168–2174, 2001.

[19] G.Alici and B. Shirinzadeh. Kinematics and stiffness analyses of a flexure-jointed planar micromanipulation system for a decoupled compliant motion. In *Proceedings of the 2003 IEEE/RSJ Intl. Conference on Intelligent Robots and Systems*, Las Vegas, NV, October 2003.

[20] E. Amatucci, N.G. Dagalakis, J.A. Kramar, and F.E. Scire. Performance evaluation of a parallel cantilever biaxial micropositioning stage. In *Proc. of the American Society of Precision Engineering, 15th Annual Meeting*, Scottsdale, Arizona, 2000.

[21] N.G. Dagalakis, J.A. Kramar, E. Amatucci, and R. Bunch. Kinematic modeling and analysis of a planar micropositioner. In *Proc. of the American Society of Precision Engineering, 16th Annual Meeting*, Crystal City, Virginia, 2001.

[22] J.J. Gorman, N.G. Dagalakis, and B.G. Boone. Multi-loop control of a nanopositioning mechanism for ultra-precision beam steering. In *Free-Space Laser Communication and Active Laser Illumination III, SPIE Vol. 5160*, pages 170–181, San Diego, CA, 2003.

[23] B.G. Boone, R.S. Bokulic, G.B. Andrewsa, R.L. McNutt, Jr., and N. Dagalakis. Optical and microwave communications system conceptual design for a realistic interstellar explorer. In *Proceedings of the 47th Annual SPIE Meeting*, Seattle, WA, July 2002.